Title

Dose-dependent white matter damage after brain radiotherapy

Journal

Radiotherapy and Oncology, 121(2)

ISSN

0167-8140

Authors

Connor, Michael

Karunamuni, Roshan

McDonald, Carrie

et al.

Publication Date

2016-11-01

DOI

10.1016/j.radonc.2016.10.003

Peer reviewed

HHS Public Access

Author manuscript

Radiother Oncol. Author manuscript; available in PMC 2017 November 01.

Published in final edited form as:

Radiother Oncol. 2016 November ; 121(2): 209–216. doi:10.1016/j.radonc.2016.10.003.

Dose-Dependent White Matter Damage After Brain Radiotherapy

Michael Connor, BS[a], **Roshan Karunamuni, PhD**[a,e], **Carrie McDonald, PhD**[a,c,e], **Nathan White, PhD**[b,e], **Niclas Pettersson, PhD**[a], **Vitali Moiseenko, PhD**[a], **Tyler Seibert, MD, PhD**[a,e], **Deborah Marshall, BS**[a], **Laura Cervino, PhD**[a], **Hauke Bartsch, PhD**[b,e], **Joshua Kuperman, PhD**[b,e], **Vyacheslav Murzin, PhD**[a], **Anitha Krishnan, PhD**[b,e], **Nikdokht Farid, MD**[b,e], **Anders Dale, PhD**[b,c,d,e], and **Jona Hattangadi-Gluth, MD**[a,e]

[a]Department of Radiation Medicine and Applied Sciences, University of California San Diego, United States

[b]Department of Radiology, University of California San Diego, United States

[c]Department of Psychiatry, University of California San Diego, United States

[d]Department of Neurosciences, University of California San Diego, United States

[e]Multimodal Imaging Laboratory, University of California San Diego, United States

Abstract

Background and Purpose—Brain radiotherapy is limited in part by damage to white matter, contributing to neurocognitive decline. We utilized diffusion tensor imaging (DTI) with multiple b-values (diffusion weightings) to model the dose-dependency and time course of radiation effects on white matter.

Materials and Methods—Fifteen patients with high-grade gliomas treated with radiotherapy and chemotherapy underwent MRI with DTI prior to radiotherapy, and after months 1, 4-6, and 9-11. Diffusion tensors were calculated using three weightings (high, standard, and low b-values) and maps of fractional anisotropy (FA), mean diffusivity (MD), axial diffusivity ($\lambda_{\parallel}$), and radial diffusivity ($\lambda_{\perp}$) were generated. The region of interest was all white matter.

Results—MD, $\lambda_{\parallel}$, and $\lambda_{\perp}$increased significantly with time and dose, with corresponding decrease in FA. Greater changes were seen at lower b-values, except for FA. Time-dose interactions were highly significant at 4-6 months and beyond ($p < .001$), and the difference in dose response between high and low b-values reached statistical significance at 9-11 months for MD, $\lambda_{\parallel}$, and $\lambda_{\perp}$ ($p < .001$, $p < .001$, $p = .005$ respectively) as well as at 4-6 months for $\lambda_{\parallel}$ ($p = .04$).

Corresponding Author: Jona A. Hattangadi-Gluth, MD, Department of Radiation Medicine and Applied Sciences, 3855 Health Sciences Drive, La Jolla, CA 92093, jhattangadi@ucsd.edu, (858) 822-6040 / (858) 246-1505 (fax).

Conclusions—We detected dose-dependent changes across all doses, even <10 Gy. Greater changes were observed at low b-values, suggesting prominent extracellular changes possibly due to vascular permeability and neuroinflammation.

Keywords

diffusion tensor imaging; MRI; white matter; Radiotherapy; b-value; radiation

Introduction

Radiotherapy (RT) is a mainstay of treatment for primary and metastatic brain tumors, but limited by damage to healthy brain tissue, with corresponding neurocognitive decline seen in a majority of patients [1]. Radiation-induced cognitive impairment manifests with acute (days to weeks after RT), early delayed (1-6 months after RT and often reversible), and late delayed effects (6 months or more after RT and usually irreversible and progressive). Late delayed effects include decreases in memory and executive functioning, among other deficits, and can be devastating for patients and their quality of life [2]. The pathogenesis of this process is multifactorial but driven in part by vascular injury, white matter damage with resulting demyelination or axonal injury, and neuroinflammation.

Diffusion-weighted imaging (DWI) is a sensitive non-invasive technique that measures diffusion of water at the cellular level. Diffusion tensor imaging (DTI) is an extension of DWI that depicts the overall motion of water as an ellipse using a tensor model, with quantitative DTI metrics allowing the study of white matter [3]. Previous studies have used standard DTI to investigate the effects of radiation on normal appearing brain white matter. One group concluded that DTI metrics were only sensitive to RT-related changes above 45-50 Gy [4], while others found changes at doses as low as 5-15 Gy [5] and dose-dependent changes over time [6]. Other studies have found DTI metrics to predict clinical outcomes, i.e., early diffusion changes in the parahippocampal cingulum were predictive of late decline in verbal recall [7,8].

These prior studies used DTI with a standard b-value of 1000 s/mm^2. In DTI, the b-value is a composite measure of imaging parameters and represents the degree of diffusion weighting in the image. At high b-values (> 2000 s/mm^2), the rate of diffusion signal decay suggests a two-compartment model wherein each voxel contains two apparent diffusion coefficients – one attributed to the intracellular axonal compartment in which diffusion is referred to as slow or restricted, and one to the extracellular compartment in which diffusion is referred to as fast or hindered [9,10]. In this model, DTI is weighted towards the slow compartment at high b-values and towards the fast compartment at low b-values.

Because of its greater sensitivity to intra-axonal white matter, high b-value DTI has been used to better understand the nature of white matter changes in various brain disorders including Alzheimer's disease [11], schizophrenia [12], multiple sclerosis [13], autism [14], and stroke [15]. Low b-value imaging [16] and other DTI methods that are sensitive to water diffusion in the extracellular space have revealed biologic processes involved in white matter maturation [17] and the role of increased extracellular volume and neuroinflammation in schizophrenia and Parkinson's disease [18,19]. Therefore, techniques preferentially probing

intra-axonal or extracellular environments have improved our understanding of disease-specific biological changes in the brain.

Given the complicated effect of radiation on both axonal integrity and the extra-axonal white matter environment, we sought to use multi b-value DTI to study the dose-dependency and time course of radiation-induced white matter changes in patients with high grade glioma.

Materials and Methods

Study Design

From January 2011 to December 2013, 32 patients with primary high-grade glioma treated with fractionated brain RT underwent advanced multi b-value diffusion imaging [10]. Fifteen patients met criteria of imaging at the required time points: pre-RT, 1 month post-RT, 4-6 months post-RT, and 9-11 months post-RT. All patients were treated to 60 Gy in 30 fractions except for two: one was treated to 40.05 Gy in 15 fractions, and the other to 59.4 Gy in 33 fractions. These schedules were converted to a total equivalent dose in standard 2 Gy fractionation using biologically equivalent dose principles [20] and an α/β ratio of 2 Gy [21]. Treatment and demographic factors are shown in Table 1. This study was approved by our institutional review board.

MRI Acquisition

MR imaging was performed on a 3T Signa Excite HDx scanner (GE Healthcare, Milwaukee, Wisconsin) equipped with an 8-channel head coil. The imaging protocol included a 3D volumetric T1-weighted inversion recovery spoiled gradient-echo sequence (TE, 2.8 ms; TR, 6.5 ms; TI, 450 ms) and a 3D T2-weighted FLAIR sequence (TE, 126 ms; TR, 6000 ms; TI, 1863 ms). Diffusion data were acquired with a single-shot pulsed-field gradient spin-echo-planar imaging sequence (TE, 96 ms; TR, 17 s) at b = 0, 500, 1500, and 4000 s/mm^2, with 1, 6, 6, and 15 unique gradient directions for each b-value, respectively.

Image Processing and Registration

All image data were preprocessed using in-house algorithms developed in MATLAB (Mathworks, Natick, Massachusetts). Anatomical scans were corrected for distortions due to gradient nonlinearities. Diffusion scans were corrected for spatial distortions associated with susceptibility and eddy currents. Within each time-point, diffusion data was co-registered to the T1 and T2 scans. Between time-points, a computed average of the T1-weighted and T2-weighted sequences were used to co-register images from each time point to the baseline dataset. Planning CT and radiation dose maps were co-registered to the baseline T1. Registrations were performed using rigid-body transformation based on mutual information and were visually inspected for accuracy.

Region of Interest

The region of interest included all white matter (Fig 1a), excluding tumor, tumor bed, surgical cavity, and surgical scars which were manually censored on each patient. A white matter mask was computed from the T1-weighted sequence at the baseline time-point using automatic segmentation software (Fig 1a) [22]. In order to avoid partial volume effects from

gray matter and CSF at the edges of the volume, the mask was shrunk to its 6-connected voxels (voxels whose 6 face neighbors were also white matter) (Fig 1b). A post-hoc analysis was performed to study the effect of edema on observed trends by further excluding voxels identified as edema based on T2 FLAIR hyperintensity (Fig 1c). Within these ROIs, volumes were further divided into dose bins of 0-10 Gy, 10-20 Gy, 20-30 Gy, 40-50 Gy, and >50 Gy.

DTI Analysis

The diffusion tensor at each time point was calculated using mono-exponential fitting and three diffusion weightings: high b-value (b=0, 4000), standard b-value (b=0, 500, 1500), and low b-value (b=0, 500). The terms “high”, “standard”, and “low” subsequently refer to these diffusion tensor data. Since our protocol does not acquire data at b=1000 s/mm^2, we performed a mono-exponential fit using three points (b=0, 500, 1500) to approximate this standard b-value.

We analyzed four main diffusion metrics, each computed as a map at each time-point. The diffusion process in each voxel is approximated by an ellipsoid defined by three perpendicular axes or eigenvectors - the principal long axis λ_1, and the smaller axes of width and depth, λ_2 and λ_3 [23]. Mean diffusivity (MD) is a rotationally invariant measure of the average mobility of water molecules. It is expressed in mm^2/s and calculated as an average of the three eigenvalues, $(\lambda_1 + \lambda_2 + \lambda_3) / 3$. Fractional anisotropy (FA) ranges from 0 to 1 as an expression of the degree of directional bias of diffusion. Diffusion along λ_1 (along the axon in white matter) is termed axial, or longitudinal diffusivity, referred to here as $\lambda_\parallel$. Radial, or perpendicular diffusivity, is defined as $\lambda_\perp = (\lambda_2 + \lambda_3) / 2$ and occurs perpendicular to axonal orientation. Classically, preclinical studies have shown $\lambda_\parallel$ is a marker for axonal degeneration and $\lambda_\perp$ is a marker for demyelination [24,25].

Statistical Analysis

Statistical analysis was performed with R [26]. Descriptive statistics of MD, FA, $\lambda_\parallel$, and $\lambda_\perp$ were obtained for each region of interest and dose bin. Two-tailed paired Student's t-tests were used to determine statistically significant differences between b-values, between white matter and white matter excluding edema, and among the time points. Results were considered significant with two-tailed $p < 0.05$, with Bonferroni correction for multiple comparisons.

We further used R and *lme4* [27] to perform linear mixed effects analyses of the relationship between b-value, time, RT dose, and percent change in each DTI parameter. As fixed effects, we included time and a time-dose interaction term, and further interacted each of these terms with b-value. We suppressed the fixed effects intercept as this yielded estimates of absolute change at each time point, rather than relative values. To control for correlated observations within subjects, we tested a subject-specific random intercept.

$$[\text{DTI parameter}] \sim 0 + b\text{value:time} + b\text{value:time:dose} + (1|\text{patient})$$

Model selection was based on likelihood ratio tests of the full model above versus reduced models. Coefficients at high and low b-values were compared using manually specified contrasts with *multcomp* [28] in R.

Results

Figure 2 shows percent change of DTI metrics across time and RT dose among the three b-values, with raw values shown in Supplementary Table 1. MD increased consistently over time, with a greater rate of change at higher doses and a greater percent change at lower b-values. Early changes at 1 month were not statistically significant in any dose bin. Changes at 4-6 months were significant above 30 Gy and changes at 9-11 months were significant at doses >10 Gy. Differences between high and low b-values were significant by 1 month at 40-50 Gy, by 4-6 months at >30 Gy, and by 9-11 months at >20 Gy.

FA decreased over time with greater rate of change at higher RT doses, and greater percent change at high compared to standard and low b-values. Changes in FA were found to be significant at the lowest dose bin (<10 Gy) over time. Standard b-value changes were the greatest up to 30 Gy while above 40 Gy, high b-value changes became greatest. Differences between high and low b-value were significant at doses above 30 Gy.

There were similar trends in $\lambda_{\parallel}$ as in MD, showing progressive increase with time and dose. At doses >50 Gy after 9-11 months, $\lambda_{\parallel}$ increased 18.0% at high b-value, 23.9% at standard b-value, and 34.1% at low b-value ($p < .001$). Changes at 1 month were significant above 50 Gy. Changes at 4-6 months were significant above 30 Gy and changes at 9-11 months were significant at doses >10 Gy. Differences between high and low b-values were significant by 1 month at >50 Gy, by 4-6 months at >30 Gy, and by 9-11 months at >20 Gy.

Changes in $\lambda_{\perp}$ were likewise greatest at low b-value, with standard and high b-value changes similar to one another. At doses >50 Gy after 9-11 months, $\lambda_{\perp}$ increased 39.2% at high b-value, 57.1% at standard b-value, and 55.3% at low b-value ($p < .001$). Changes at 1 month were significant above 40 Gy. Changes at 4-6 months were significant above 30 Gy, and changes at 9-11 months were significant at all doses. Differences between high and low b-values were significant by 1 month above 40 Gy, by 4-6 months above 30 Gy, and by 9-11 months above 20 Gy. The overall magnitude of change over all doses was greater in $\lambda_{\perp}$ compared with $\lambda_{\parallel}$.

All time-only coefficients were not significant ($p > .05$). Table 2 shows time-dose interaction coefficients and significance at each post-RT time point and b-value, and these are plotted in Figure 3 as percent change from baseline per Gy. For these time-dose interaction coefficients, all are significant at 1 month and by 4-6 months are highly significant at $p < .001$ (Fig 3, Table 2). For MD, $\lambda_{\parallel}$ and $\lambda_{\perp}$ the predicted percent change per Gy increases as b-value decreases, with the sole exception of the standard vs. low b-value $\lambda_{\perp}$ at 9-11 months. Predicted percent changes of $\lambda_{\perp}$ are greater than $\lambda_{\parallel}$. The trend for FA is reversed, showing a greater magnitude of change with increasing b-value. Differences in dose response between high and low b-values reached significance at 9-11 months for MD, $\lambda_{\parallel}$, and $\lambda_{\perp}$ ($p < .001$, $p < .001$, $p = .005$ respectively) as well as at 4-6 months for $\lambda_{\parallel}$ ($p = .04$).

Recognizing that the signal at lower b-values is more weighted towards fast, extracellular water, we sought to further sub-divide our ROI based on T2 FLAIR hyperintensity. This would help to determine if our results were driven by edema and if the finding of increased change in low b-value metrics held true in normal appearing white matter exclusive of identifiable edema. The data show little difference at 9-11 months between the two ROIs of white matter vs. white matter excluding FLAIR hyperintensity (Fig 4). The only significant differences between the two ROIs were for FA at low and standard b-value >50 Gy ($p = .008$ and $p = .04$ respectively). At 4-6 months, the vast majority of comparisons are again insignificant, with only changes at doses >50 Gy in FA as exceptions. At 1 month, all comparisons were insignificant.

Discussion

To our knowledge, this is the first study to utilize multi b-value diffusion imaging to analyze the dose-dependence and biology of radiation-induced white matter damage over time. We detected progressive dose-dependent change in all quantitative DTI metrics (MD, FA, $\lambda_{\parallel}$, and $\lambda_{\perp}$) across all b-values. We also found greater changes at lower b-values suggesting more prominent biologic changes in the extracellular environment. These data remained largely unchanged by the exclusion of regions of edema, suggesting our findings are driven by diffusion changes in normal appearing white matter.

Similar to our results, earlier studies using DTI to investigate radiation-induced white matter damage found decreases in FA [4,29-31], and increases in MD [4,30]. Results varied with respect to dose-dependence, with one report of a linear relationship [29] and another noting a 45-50 Gy threshold for detection of DTI metric change [4]. Here we report a linear dose-dependent decrease in FA and increase in MD consistent with general trends in previous studies. We found no threshold for change, reversal, or plateau. Our model showed a linear relationship between dose and changes in MD and FA, indicating dose-dependent progressive damage to white matter. Furthermore, our data suggests it takes longer to detect significant low dose changes. White matter receiving low doses of 10-20 Gy showed significant diffusion changes at 9-11 months, while areas receiving >30 Gy were significant at 4-6 months. This also implies that low dose white matter changes can be reliably measured in brain tissue.

We also found dose-dependent and progressive increase in $\lambda_{\parallel}$ and $\lambda_{\perp}$. Change in $\lambda_{\parallel}$ is considered a marker of axonal degeneration. Increased $\lambda_{\parallel}$ has been found with axonal damage in amyotrophic lateral sclerosis (ALS) [32,33], multiple sclerosis (MS) [34], and in animal models of myelin deficiency [35,36]. On the other hand, decreases in $\lambda_{\parallel}$ have also been associated with axonal injury in preclinical studies [24]. Reports of $\lambda_{\parallel}$ changes in white matter following radiation are accordingly mixed, with studies showing either increase or decrease [6,7]. It is clear, however, that change in $\lambda_{\parallel}$ is associated with pathologies causing axonal damage. Increased $\lambda_{\perp}$ is a marker for myelin damage in preclinical models [25,37] as well as in ALS [32,38], MS [34,39], and autism [40]. Indeed, diffusion imaging studies of radiation damage to white matter have found increased $\lambda_{\perp}$ [6,7]. The utility of $\lambda_{\parallel}$ and $\lambda_{\perp}$ as markers of axonal and myelin injury, respectively, is not confounded by the simultaneous presence of both pathologies [24].

In the current study, the magnitude of change in $\lambda_{\perp}$ was greater than $\lambda_{\parallel}$, consistent with prior studies and indicating progressive demyelination as the likely predominant change. The magnitude of change in both $\lambda_{\parallel}$ and $\lambda_{\perp}$ was also greater at low b-value. Given the larger contribution from extracellular diffusion activities at low b-value, greater increases in $\lambda_{\parallel}$ at low b-value may indicate reduced extracellular diffusion restrictions due to the absence of compact myelin [36]. FA, as a general marker for white matter integrity, showed dose-dependent decrease over time, with greater change at high b-values. FA is a summary measure calculated from the three eigenvalues, so more specific information on changes in the diffusion tensor is available from $\lambda_{\parallel}$ and $\lambda_{\perp}$. Nevertheless, these data are consistent with the progressive white matter damage seen after radiation in other studies [4,29-31].

The greater changes at low b-value suggest more prominent microstructural changes in the extracellular environment possibly due to vascular permeability, a known factor in radiation injury, and neuroinflammation. The relationship between the persistent extra-axonal radiation-induced processes and intra-axonal diffusion changes seen in this study is unclear. However, chronic inflammation has been shown to drive axonal degeneration in MS [41], and similarly, analysis using free-water diffusion has revealed the role of neuroinflammation in early onset schizophrenia, perhaps leading to more severe later white matter degeneration [42]. Indeed, an inflammatory response to irradiation is likely one of many factors in the pathogenesis of radiation-induced brain injury, and preclinical data suggests anti-inflammatory treatment may combat radiation-induced cognitive decline [43].

Our data suggests that, in terms of microstructural damage, even low dose to white matter may not be “safe”. While the diffusion changes seen here have not yet been correlated with neurocognitive injury, others studies have made this correlation [7,8,44], supporting the utility of diffusion metrics to measure white matter injury. As of yet, for fractionated partial brain RT, there are no clear dose constraints for subcortical white matter. Maximum dose constraints for brain “parenchyma” do not distinguish between cortex, white matter, and other deep gray matter structures. Characterizing radiation response in the brain using imaging biomarkers, such as subcortical white matter in this study, or hippocampal or cortical measures in others [45,46], is a critical step in developing more refined techniques to understand radiation-induced brain injury. This could inform novel techniques in brain radiotherapy planning [47] to allow for better sparing of critical brain structures [48], with the potential to reduce neurocognitive sequelae.

Limitations to our study include its retrospective nature and potential confounding effects from chemotherapy or surgery. Our study lacks histopathological outcomes, though preclinical data show a clear correlation with changes in diffusivity metrics and white matter damage [24]. We also followed patients for up to 9-11 months, although radiation damage is known to evolve over several years, so future studies should evaluate chronic white matter changes after one-year post radiation. Studies correlating the changes seen here with post-RT cognitive decline are underway at our institution.

In conclusion, we found progressive dose-dependent change in MD, FA, $\lambda_{\parallel}$, and $\lambda_{\perp}$ in patients up to 9-11 months following RT for high grade gliomas. We also found increased sensitivity of low b-value DTI metrics to radiation-induced damage in normal appearing

white matter. These findings suggest that multiple pathological processes are involved in RT-induced damage, including demyelination, axonal loss, and vascular permeability or neuroinflammation, with greater increase in extracellular diffusion processes. DTI with different b-values can be used to probe different cellular microstructures, allowing further characterization of radiation injury in white matter.

Supplementary Material

Refer to Web version on PubMed Central for supplementary material.

Acknowledgments

None

Funding: This work was partially supported by the following grants: National Institutes of Health (KL2RR031978, KL2TR00099, UL1TR000100 to J.H-G.); American Cancer Society (Pilot Award ACS-IRG #70-002 to J.H-G.); National Science Foundation Grant (1430082 to N.W.); American Cancer Society Research (Scholar Grant RSG-15-229-01-CCE to C.M.); National Cancer Institute Cancer Center (Specialized Grant P30CA023100 to C.M., J.H-G.) No study sponsor was directly involved in study design; in the collection, analysis and interpretation of data; in the writing of the manuscript; or in the decision to submit the manuscript for publication.

Conflict of Interest: Dr. Hattangadi-Gluth has a research grant from Varian Medical Systems, unrelated to the current study. Dr. Dale receives funding through research agreements with General Electric Healthcare, and Medtronic, unrelated to the current study. Dr. Moiseenko reports prior honorarium and travel fees from Varian Medical Systems for a talk outside the submitted work.

References

1. Crossen JR, Garwood D, Glatstein E, Neuwelt EA. Neurobehavioral sequelae of cranial irradiation in adults: a review of radiation-induced encephalopathy. J Clin Oncol. 1994; 12:627–42. [PubMed: 8120563]
2. Frost M, Sloan J. Quality of life measurements: A soft outcome - Or is it? Am J Manag Care. 2002; 8:S574–9. [PubMed: 12512981]
3. Basser PJ, Mattiello J, LeBihan D. MR diffusion tensor spectroscopy and imaging. Biophys J. 1994; 66:259–67. DOI: 10.1016/S0006-3495(94)80775-1 [PubMed: 8130344]
4. Haris M, Kumar S, Raj MK, et al. Serial diffusion tensor imaging to characterize radiation-induced changes in normal-appearing white matter following radiotherapy in patients with adult low-grade gliomas. Radiat Med - Med Imaging Radiat Oncol. 2008; 26:140–50. DOI: 10.1007/s11604-007-0209-4
5. Ravn S, Holmberg M, Sørensen P, Frøkjær JB, Carl J. Differences in supratentorial white matter diffusion after radiotherapy--new biomarker of normal brain tissue damage? Acta Oncol (Madr). 2013; 52:1314–9. DOI: 10.3109/0284186X.2013.812797
6. Nagesh V, Tsien CI, Chenevert TL, et al. Radiation-Induced Changes in Normal-Appearing White Matter in Patients With Cerebral Tumors: A Diffusion Tensor Imaging Study. Int J Radiat Oncol Biol Phys. 2008; 70:1002–10. DOI: 10.1016/j.ijrobp.2007.08.020 [PubMed: 18313524]
7. Chapman CH, Nagesh V, Sundgren PC, et al. Diffusion tensor imaging of normal-appearing white matter as biomarker for radiation-induced late delayed cognitive decline. Int J Radiat Oncol Biol Phys. 2012; 82:2033–40. DOI: 10.1016/j.ijrobp.2011.01.068 [PubMed: 21570218]
8. Chapman CH, Zhu T, Nazem-Zadeh M, et al. Diffusion tensor imaging predicts cognitive function change following partial brain radiotherapy for low-grade and benign tumors. Radiother Oncol. 2016; 120:234–40. DOI: 10.1016/j.radonc.2016.06.021 [PubMed: 27418525]
9. Mulkern RV, Zengingonul HP, Robertson RL, et al. Multi-component Apparent Diffusion Coefficients in Human Brain: Relationship to Spin-Lattice Relaxation. 1999; 12:51–62.

10. White NS, Leergaard TB, D'Arceuil H, Bjaalie JG, Dale AM. Probing tissue microstructure with restriction spectrum imaging: Histological and theoretical validation. Hum Brain Mapp. 2013; 34:327–46. DOI: 10.1002/hbm.21454 [PubMed: 23169482]
11. Yoshiura T, Mihara F, Tanaka A, et al. High b value diffusion-weighted imaging is more sensitive to white matter degeneration in Alzheimer's disease. Neuroimage. 2003; 20:413–9. DOI: 10.1016/S1053-8119(03)00342-2 [PubMed: 14527601]
12. Baumann PS, Cammoun L, Conus P, et al. High b-value diffusion-weighted imaging: a sensitive method to reveal white matter differences in schizophrenia. Psychiatry Res. 2012; 201:144–51. DOI: 10.1016/j.pscychresns.2011.08.003 [PubMed: 22386971]
13. Assaf Y, Ben-Bashat D, Chapman J, et al. High b-value q-space analyzed diffusion-weighted MRI: Application to multiple sclerosis. Mrm. 2002; 47:115–26. DOI: 10.1002/mrm.10040 [PubMed: 11754450]
14. Ben Bashat D, Kronfeld-Duenias V, Zachor DA, et al. Accelerated maturation of white matter in young children with autism: A high b value DWI study. Neuroimage. 2007; 37:40–7. DOI: 10.1016/j.neuroimage.2007.04.060 [PubMed: 17566764]
15. Brugières P, Thomas P, Maraval A, et al. Water diffusion compartmentation at high b values in ischemic human brain. AJNR Am J Neuroradiol. 2004; 25:692–8. [PubMed: 15140706]
16. Takahara T, Kwee TC. Low b-value diffusion-weighted imaging: Emerging applications in the body. J Magn Reson Imaging. 2012; 35:1266–73. DOI: 10.1002/jmri.22857 [PubMed: 22359279]
17. Hui ES, Cheung MM, Chan KC, Wu EX. B-value dependence of DTI quantitation and sensitivity in detecting neural tissue changes. Neuroimage. 2010; 49:2366–74. DOI: 10.1016/j.neuroimage.2009.10.022 [PubMed: 19837181]
18. Pasternak O, Westin CF, Bouix S, et al. Excessive Extracellular Volume Reveals a Neurodegenerative Pattern in Schizophrenia Onset. J Neurosci. 2012; 32:17365–72. DOI: 10.1523/JNEUROSCI.2904-12.2012 [PubMed: 23197727]
19. Ofori E, Pasternak O, Planetta PJ, et al. Longitudinal changes in free-water within the substantia nigra of Parkinson's disease. Brain. 2015; 138:2322–31. DOI: 10.1093/brain/awv136 [PubMed: 25981960]
20. Bruzzaniti V, Abate A, Pedrini M, Benassi M, Strigari L. IsoBED: a tool for automatic calculation of biologically equivalent fractionation schedules in radiotherapy using IMRT with a simultaneous integrated boost (SIB) technique. J Exp Clin Cancer Res. 2011; 30:52.doi: 10.1186/1756-9966-30-52 [PubMed: 21554675]
21. Fowler JF. The linear-quadratic formula and progress in fractionated radiotherapy. Br J Radiol. 1989; 62:679–94. DOI: 10.1259/0007-1285-62-740-679 [PubMed: 2670032]
22. Fischl B, Salat DH, Busa E, et al. Whole brain segmentation: Automated labeling of neuroanatomical structures in the human brain. Neuron. 2002; 33:341–55. DOI: 10.1016/S0896-6273(02)00569-X [PubMed: 11832223]
23. Alexander AL, Lee JE, Lazar M, Field AS. Diffusion tensor imaging of the brain. Neurotherapeutics. 2007; 4:316–29. DOI: 10.1016/j.nurt.2007.05.011 [PubMed: 17599699]
24. Song SK, Sun SW, Ju WK, et al. Diffusion tensor imaging detects and differentiates axon and myelin degeneration in mouse optic nerve after retinal ischemia. Neuroimage. 2003; 20:1714–22. DOI: 10.1016/j.neuroimage.2003.07.005 [PubMed: 14642481]
25. Song SK, Sun SW, Ramsbottom MJ, et al. Dysmyelination Revealed through MRI as Increased Radial (but Unchanged Axial) Diffusion of Water. Neuroimage. 2002; 17:1429–36. DOI: 10.1006/nimg.2002.1267 [PubMed: 12414282]
26. R Core Team. Vienna, Australia: 2015. R: A Language and Environment for Statistical Computing. https://www.r-project.org n.d
27. Bates D, Mächler M, Bolker B, Walker S. Fitting Linear Mixed-Effects Models Using lme4. J Stat Softw. 2015; 67doi: 10.18637/jss.v067.i01
28. Hothorn T, Bretz F, Westfall P. Simultaneous inference in general parametric models. Biometrical J. 2008; 50:346–63. DOI: 10.1002/bimj.200810425
29. Qiu D, Leung LHT, Kwong DLW, Chan GCF, Khong PL. Mapping radiation dose distribution on the fractional anisotropy map: Applications in the assessment of treatment-induced white matter

injury. Neuroimage. 2006; 31:109–15. DOI: 10.1016/j.neuroimage.2005.12.007 [PubMed: 16448821]

30. Khong PL, Kwong DLW, Chan GCF, et al. Diffusion-tensor imaging for the detection and quantification of treatment-induced white matter injury in children with medulloblastoma: a pilot study. AJNR Am J Neuroradiol. 2003; 24:734–40. [PubMed: 12695214]
31. Welzel T, Niethammer A, Mende U, et al. Diffusion tensor imaging screening of radiation-induced changes in the white matter after prophylactic cranial irradiation of patients with small cell lung cancer: first results of a prospective study. AJNR Am J Neuroradiol. 2008; 29:379–83. DOI: 10.3174/ajnr.A0797 [PubMed: 17974610]
32. Metwalli NS, Benatar M, Nair G, et al. Utility of axial and radial diffusivity from diffusion tensor MRI as markers of neurodegeneration in amyotrophic lateral sclerosis. Brain Res. 2010; 1348:156–64. DOI: 10.1016/j.brainres.2010.05.067 [PubMed: 20513367]
33. Wong JCT, Concha L, Beaulieu C, et al. Spatial profiling of the corticospinal tract in amyotrophic lateral sclerosis using diffusion tensor imaging. J Neuroimaging. 2007; 17:234–40. DOI: 10.1111/j.1552-6569.2007.00100.x [PubMed: 17608909]
34. Roosendaal S, Guerts J, Vrenken H, et al. Regional DTI differences in multiple sclerosis patients. Neuroimage. 2009; 44:1397–403. DOI: 10.1016/j.neuroimage.2008.10.026 [PubMed: 19027076]
35. Gulani V, Webb AG, Duncan ID, Lauterbur PC. Apparent diffusion tensor measurements in myelin-deficient rat spinal cords. Magn Reson Med. 2001; 45:191–5. DOI: 10.1002/1522-2594(200102)45:2<191::AID-MRM1025>3.0.CO;2-9 [PubMed: 11180424]
36. Tyszka JM, Readhead C, Bearer EL, Pautler RG, Jacobs RE. Statistical diffusion tensor histology reveals regional dysmyelination effects in the shiverer mouse mutant. Neuroimage. 2006; 29:1058–65. DOI: 10.1016/j.neuroimage.2005.08.037 [PubMed: 16213163]
37. Song SK, Yoshino J, Le TQ, et al. Demyelination increases radial diffusivity in corpus callosum of mouse brain. Neuroimage. 2005; 26:132–40. DOI: 10.1016/j.neuroimage.2005.01.028 [PubMed: 15862213]
38. Cosottini M, Giannelli M, Siciliano G, et al. Diffusion-tensor MR imaging of corticospinal tract in amyotrophic lateral sclerosis and progressive muscular atrophy. Radiology. 2005; 237:258–64. DOI: 10.1148/radiol.2371041506 [PubMed: 16183935]
39. Tachibana Y, Obata T, Yoshida M, et al. Analysis of normal-appearing white matter of multiple sclerosis by tensor-based two-compartment model of water diffusion. Eur Radiol. 2015; 25:1701–7. DOI: 10.1007/s00330-014-3572-4 [PubMed: 25577520]
40. Alexander AL, Lee JE, Lazar M, et al. Diffusion tensor imaging of the corpus callosum in Autism. Neuroimage. 2007; 34:61–73. DOI: 10.1016/j.neuroimage.2006.08.032 [PubMed: 17023185]
41. Frischer JM, Bramow S, Dal-Bianco A, et al. The relation between inflammation and neurodegeneration in multiple sclerosis brains. Brain. 2009; 132:1175–89. DOI: 10.1093/brain/awp070 [PubMed: 19339255]
42. Pasternak O, Westin CF, Dahlben B, Bouix S, Kubicki M. The extent of diffusion MRI markers of neuroinflammation and white matter deterioration in chronic schizophrenia. Schizophr Res. 2015; 161:113–8. DOI: 10.1016/j.schres.2014.07.031 [PubMed: 25126717]
43. Greene-Schloesser D, Robbins ME, Peiffer AM, et al. Radiation-induced brain injury: A review. Front Oncol. 2012; 2:1–18. DOI: 10.3389/fonc.2012.00073
44. Khong PL, Leung LHT, Fung ASM, et al. White matter anisotropy in post-treatment childhood cancer survivors: preliminary evidence of association with neurocognitive function. J Clin Oncol. 2006; 24:884–90. DOI: 10.1200/JCO.2005.02.4505 [PubMed: 16484697]
45. Karunamuni R, Bartsch H, White NS, et al. Dose-Dependent Cortical Thinning after Partial Brain Irradiation in High-Grade Glioma. Int J Radiat Oncol Biol Phys. 2016; 94:297–304. DOI: 10.1016/j.ijrobp.2015.10.026 [PubMed: 26853338]
46. Farjam R, Pramanik P, Aryal MP, et al. A radiation-induced hippocampal vascular injury surrogate marker predicts late neurocognitive dysfunction. Int J Radiat Oncol. 2015; 93:908–15. DOI: 10.1016/j.ijrobp.2015.08.014
47. Smyth, G.; Evans, PM.; Bamber, JC., et al. Radiother Oncol. 2016. Non-coplanar trajectories to improve organ at risk sparing in volumetric modulated arc therapy for primary brain tumours; p.

1-8.Joint Department of Physics at The Institute of Cancer Research and The Royal Marsden NHS Foundation Trust, London, SM2 5PT, United

48. Karunamuni RA, Moore KL, Seibert TM, et al. Radiation sparing of cerebral cortex in brain tumor patients using quantitative neuroimaging. Radiother Oncol. 2016; 118:1–6. DOI: 10.1016/j.radonc.2016.01.003 [PubMed: 26700603]

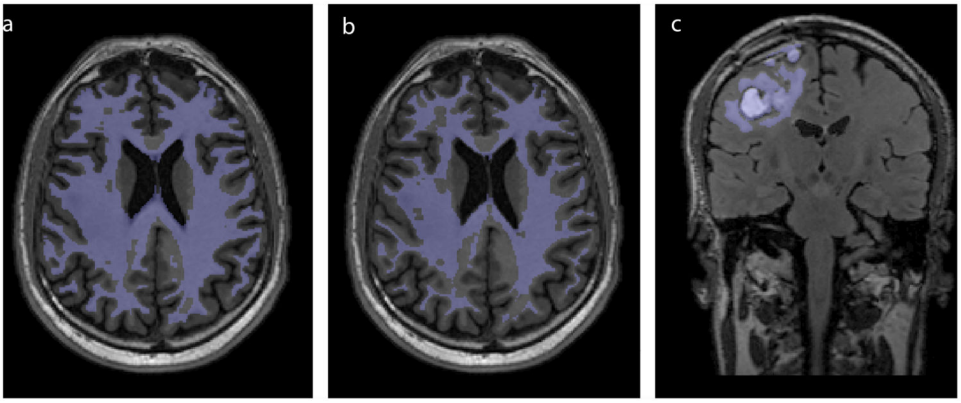

Fig 1.

a Original white matter mask. **b** Eroded 6-connected white matter. **c** FLAIR hyperintensity

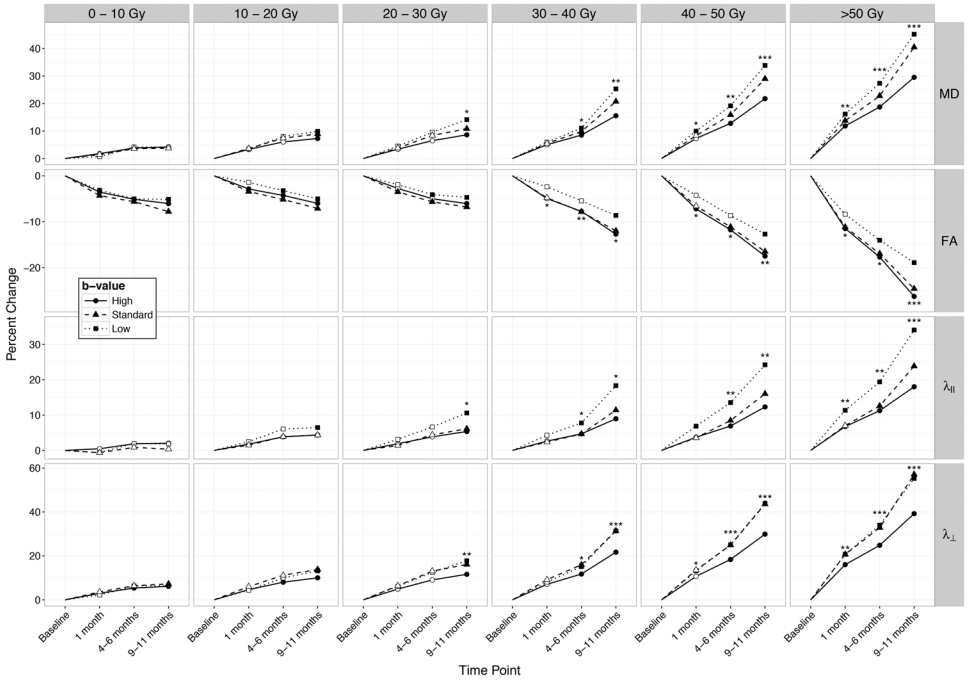

Fig 2.

Percent changes from baseline in MD, FA, $\lambda_{\parallel}$, and $\lambda_{\perp}$ for each dose bin and b-value. Hollow points: no significant change from baseline. Filled points: significant change from baseline. Asterisks: significance for paired t-tests between changes at high and low b-values at each time point (*** $p < .001$, ** $p < .01$, * $p < .05$)

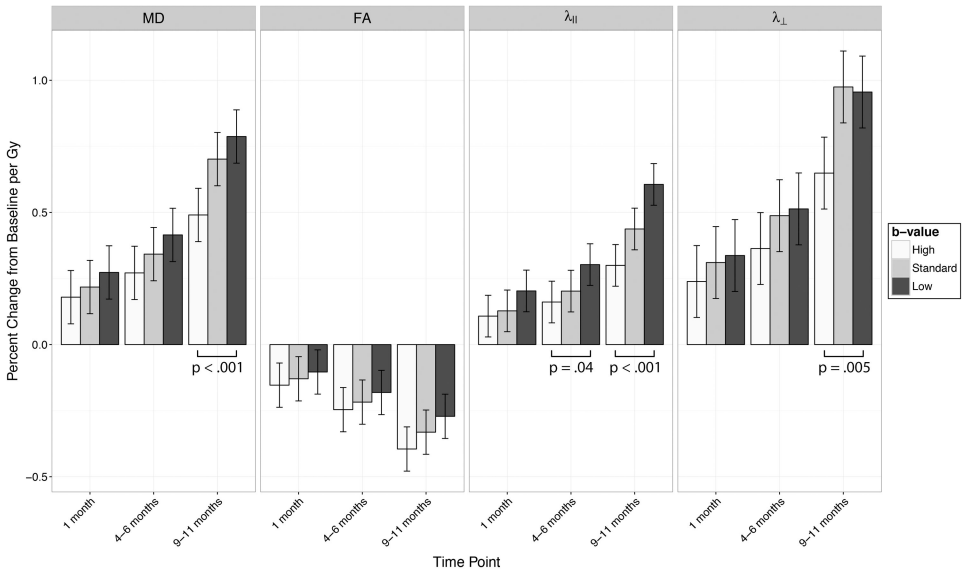

Fig 3.

Time-dose interaction coefficients at each time point and b-value. The coefficients represent percent change per Gy. Error bars represent 95% confidence intervals. Significant p-values for tests between high and low b-value coefficients are shown

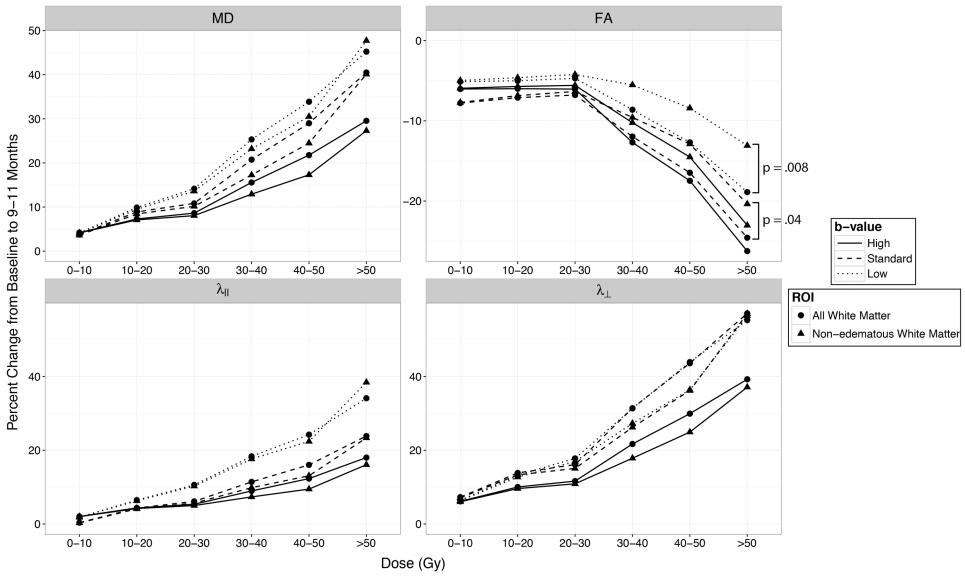

Fig 4.

Percent changes in MD, FA, $\lambda_{\parallel}$, and $\lambda_{\perp}$ for each dose bin and b-value at 9-11 months; white matter (circles) vs. white matter excluding FLAIR hyperintensity (triangles). Significant differences between ROIs are labeled

Table 1

Summary of patient characteristics.

Characteristic	Number of patients (%)
Sex	
Male	9 (60)
Female	6 (40)
Median age (y) (range)	59 (40-84)
Tumor histology	
Glioblastoma	15 (100)
Median largest dimension of preoperative tumor (cm) (range)	3.2 (1.0-5.0)
Median planning target volume (cc) (range)	170.0 (25.8-376.8)
Tumor Location	
Temporal	7 (46.7)
Frontal	4 (26.7)
Parietal	1 (6.7)
Parietotemporal	2 (13.3)
Frontoparietal	1 (6.7)
Surgery	
Gross total resection	6 (40)
Subtotal resection	9 (60)
RT dose, Gy (fraction size)	
60 (2)	13 (86.7)
59.4 (1.8)	1 (6.7)
40.05 (2.67)	1 (6.7)
Concurrent chemotherapy	
Temozolomide only	7 (46.7)
Temozolomide + vaccine trial[a]	4 (26.7)
Temozolomide + other clinical trial[b]	4 (26.7)
Adjuvant chemotherapy	
Temozolomide only	5 (26.7)
Temozolomide + other chemotherapy[c]	1 (6.7)
Temozolomide + bevacizumab	1 (6.7)
Temozolomide + other clinical trial[d]	6 (40)
Temozolomide + vaccine trial[e]	2 (13.3)

[a] Vaccine trial of activated dendritic cells (n=4)

[b] α_V integrin inhibitor trial (n=2); bevacizumab trial (n=1); trial of paclitaxel linked to poly-L-glutamic acid (n=1)

[c] rapamycin, lapatinib

[d] Gene therapy (n=1), inhibitor of poly (ADP-ribose) polymerase (n=2), small molecule tyrosine kinase inhibitor (n=1), epidermal growth factor receptor variant III-based immunotherapy (n=2)

[e] Vaccine trial of activated dendritic cells (n=2)

Table 2

Time-dose interaction coefficients and p-values at each time point and b-value. The coefficients represent percent change per Gy, and p-values test significance of the change at each time point compared to zero

Diffusion Metric	**1 month**		**4-6 months**		**9-11 months**	
b-value	**Coefficient**	**p-value**	**Coefficient**	**p-value**	**Coefficient**	**p-value**
Mean Diffusivity						
High b-value	0.179	<.001	0.271	<.001	0.490	<.001
Standard b-value	0.218	<.001	0.342	<.001	0.702	<.001
Low b-value	0.273	<.001	0.415	<.001	0.787	<.001
Fractional Anisotropy						
High b-value	-0.153	<.001	-0.246	<.001	-0.395	<.001
Standard b-value	-0.129	.002	-0.218	<.001	-0.331	<.001
Low b-value	-0.104	.015	-0.181	<.001	-0.271	<.001
Axial Diffusivity						
High b-value	0.108	.007	0.161	<.001	0.300	<.001
Standard b-value	0.128	.002	0.202	<.001	0.437	<.001
Low b-value	0.203	<.001	0.303	<.001	0.606	<.001
Radial Diffusivity						
High b-value	0.239	<.001	0.363	<.001	0.649	<.001
Standard b-value	0.310	<.001	0.488	<.001	0.975	<.001
Low b-value	0.337	<.001	0.513	<.001	0.956	<.001